Pergamon

Int. J. Heat Mass Transfer. Vol. 41, No. 3, pp. 625–634, 1998

Printed in Great Britain
0017-9310/98 $19.00+0.00

PII: S0017-9310(97)00138-5

Forced convection heat transfer from two heated blocks in pulsating channel flow

SEO YOUNG KIM and BYUNG HA KANG†

Air-conditiong and Environmental Control Laboratory, Korea Institute of Science and Technology, P.O. Box 131, Cheongryang, Seoul, 130-650, South Korea

and

JAE MIN HYUN

Department of Mechanical Engineering, Korea Advanced Institute of Science and Technology, Yusung-ku, Taejon, 305-701, Korea

(*Received* 14 *March* 1996 *and in final form* 21 *February* 1997)

Abstract—The pulsating flow and attendant heat transfer characteristics from two heated blocks in a channel have been numerically investigated. At the channel inlet, a pulsating flow U_i, i.e. $U_i = U_o(1 + A\sin\omega\tau)$, is imposed with uniform temperature T_C. The block surfaces in the channel are at constant temperature T_H. The channel walls are assumed to be adiabatic. Comprehensive time-dependent flow and temperature data are obtained and averaged over a cycle of pulsation in a periodic steady state. The effects of the important governing parameters, such as Reynolds number, *Re*, Strouhal number, *St*, pulsation amplitude, *A*, and the spacing between two blocks, w/H, on the heat transfer rate from the heated blocks and the flow behavior in the vicinity of the blocks are also investigated in detail. The results obtained indicate that the recirculation flows behind the downstream block as well as inside the inter-block region are substantially affected by Strouhal number *St* and inter-block spacing w/H. This, in turn, has a strong influence on the thermal transport from the heated blocks to the pulsating flow. The present results are also compared with those obtained for a steady non-pulsating flow, and the effect of pulsation on the transport process is scrutinized. © 1997 Elsevier Science Ltd.

1. INTRODUCTION

Rapid advances in the development of high-density, large scale-integrated chips have led to numerous miniaturized electronic devices. This trend produces the increase of thermal resistance due to such reduction of the heat dissipating path (i.e. denser packaging), and, consequently, heat from such sophisticated electronic components is excessively generated. Unless high-powered heat is effectively removed, the excessive heat generated within the electronic devices will rapidly degrade the performance of these sensitive systems. Therefore, enhancing the convective cooling of chips is a primary concern in the study of electronic packaging [1].

A review of the relevant literature will show that the convective cooling of chips has been a subject of active research over a past decade. For example, the convection cooling problem from a chip-simulated block has been tackled by Davalath and Bayazitoglu [2], Kang *et al.* [3], and Kim *et al.* [4] among others. Most of the earlier work has treated convective heat transfer under the steady non-pulsating flow in a channel, identifying the influence of important governing parameters such as the Reynolds number, the Prandtl number, and the Grashof number on the flow and thermal fields.

In response to the demands for high-performance electronic systems, several heat transfer augmentation schemes have been proposed to obtain the effective heat removal by utilizing flow modulations in recent years [5–10]. These schemes are relevant to the flow instabilities which appear naturally in a self-sustained oscillation or initiated by forced pulsation. The physics implemented in these schemes is the following: the hydrodynamic instability in a shear layer substantially increases lateral flow mixing in the channel, and has resulted in the augmentation of convective thermal transports.

The flow instability described above is quite complex for analytical treatment. In simple geometry, such as periodic groove channel and parallel plate channel, the least stable modes for a pulsation of infinitesimal magnitude may be predicted from linear stability theory [5, 11]. In actual electronic systems, however, the analytical prediction of an unstable mode cannot be easily obtained, because of the nonlinearity of the flow geometry inside an electronic device. Therefore, the alternative route is to conduct full-dress direct numerical computations, which this paper now addresses.

In this work, we will seek numerical solutions to

† Author to whom correspondence should be addressed.

NOMENCLATURE

A	oscillating amplitude of axial inlet velocity
C_p	specific heat of fluid
D_h	hydraulic diameter, $2H$ [m]
f	dimensional forcing frequency [Hz]
f_p	friction factor
h	height of block [m]
H	height of flow channel [m]
k	thermal conductivity [W m^{-1} K^{-1}]
l	length of block [m]
l_1	length of upstream section from the first block [m]
l_2	length of downstream section from the second block [m]
l_T	total length of channel [m]
L_1, L_2	dimensionless lengths, l_1/H, l_2/H
L_T	dimensionless length, l_T/H
$\overline{Nu}_m$	cycle-averaged and space-averaged Nusselt number
p	pressure
P	dimensionless pressure, $(p-p_0)/(\rho U_0^2)$
Pr	Prandtl number, v/α
Re	Reynolds number, $U_0 H/v$
St	Strouhal number, fH/U_0
t	dimensionless time, $\tau/(H/U_0)$
T	dimensional temperature [K]
T'	fluctuating part of temperature [K]
u, v	dimensional velocity components [m s^{-1}]
U, V	dimensionless velocity components, $U = u/U_0$, $V = v/U_0$
U_0	cycle averaged velocity of the inlet flow
U_i	inlet pulsating velocity, $U_i = U_0(1 + A \sin \omega\tau)$
u', v'	fluctuating part of velocity [m s^{-1}]
w	inter-block spacing [m]
x, y	dimensional axial and transverse coordinates [m]
X, Y	dimensionless axial and transverse coordinates, $X = x/H$, $Y = y/H$
x_R	reattachment length [m].

Greek symbols

α	thermal diffusivity, $k/\rho C_p$
β	Wormersley number
δ	boundary layer thickness [m]
v	kinematic viscosity [m^2 s^{-1}]
ρ	density [kg m^{-3}]
ϕ	phase [rad]
Θ	dimensionless temperature, $(T-T_C)/(T_H-T_C)$
τ	dimensional time [s]
Ψ	stream function
ω	angular velocity [s^{-1}].

Subscripts

C	cold
H	hot
n	harmonics index
o	reference
s	non-pulsating component.

the unsteady, two-dimensional, elliptic-type Navier–Stokes and energy equations. Comprehensive numerical results will describe the effects of externally-controllable parameters, i.e. the frequency of pulsation f, the amplitude of pulsation A, and the inter-block spacing w. The objective is to discuss the characteristics of pulsating flow and attendant heat transfer from two heated blocks in tandem inside a channel, and to secure an improved understanding of the role of flow pulsation on heat transport properties. The applicability of an external pulsation to the actual electronic devices is also examined and compared with results for the steady non-pulsating flow.

2. MATHEMATICAL MODEL AND NUMERICAL APPROACH

Consider a pulsating flow in a channel with two isolated, heated, blocks at uniform temperature, as shown in Fig. 1. The fluid enters the channel with a uniform velocity and temperature profile and leaves the channel carrying the heat dissipated by the heated blocks. The flow geometry models the cooling process of integrated chips of high-power densities mounted on a printed circuit board system. The two-dimensional Navier–Stokes and energy equations for unsteady, laminar, incompressible elliptic flow, are as follows, using the nondimensionalized quantities of length H, velocity U_0, time H/U_0, and temperature $T_H - T_C$:

Continuity

$$\frac{\partial U}{\partial X} + \frac{\partial V}{\partial Y} = 0. \tag{1}$$

Momentum equations

$$\frac{\partial U}{\partial t} + \frac{\partial}{\partial X}(UU) + \frac{\partial}{\partial Y}(UV) = \frac{v^*}{Re}\left(\frac{\partial^2 U}{\partial X^2} + \frac{\partial^2 U}{\partial Y^2}\right) - \frac{\partial P}{\partial X} \tag{2}$$

$$\frac{\partial V}{\partial t} + \frac{\partial}{\partial X}(UV) + \frac{\partial}{\partial Y}(VV) = \frac{v^*}{Re}\left(\frac{\partial^2 V}{\partial X^2} + \frac{\partial^2 V}{\partial Y^2}\right) - \frac{\partial P}{\partial Y}. \tag{3}$$

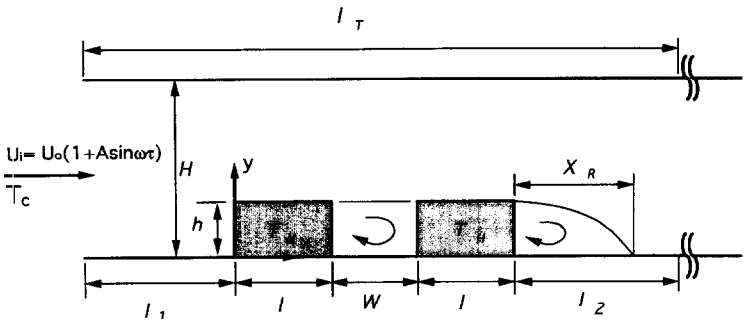

Fig. 1. Schematic configuration of the problem.

Energy equation

$$\frac{\partial\Theta}{\partial t}+\frac{\partial}{\partial X}(U\Theta)+\frac{\partial}{\partial Y}(V\Theta)=\frac{k^*}{Re\cdot Pr}\left(\frac{\partial^2\Theta}{\partial X^2}+\frac{\partial^2\Theta}{\partial Y^2}\right). \tag{4}$$

where ν^* is the ratio of the kinematic viscosity of the solid block in the domain to the kinematic viscosity of the fluid. As noted by Kim *et al.* [4], ν^* is employed for computational convenience. In the numerical treatment of the Navier–Stokes equations (2) and (3), ν^* for the blocks can be set to an infinitely large value such as 10^{30} to simulate solid blocks. As a result of this procedure, the simultaneous conjugate solutions for the solid yield close to zero velocity for the block, satisfying the no-slip boundary condition along the block surfaces. In the energy equation (4), k^* is the thermal conductivity ratio of solid to fluid. k^* is also assumed to be an infinitely large value such as 10^{30} to maintain a constant hot temperature, i.e. $\Theta = 1.0$, within the blocks.

The associated boundary conditions on U, V and Θ arise from physical considerations. The no-slip conditions at the channel walls are:

$$U(X, Y, t) = 0$$
$$V(X, Y, t) = 0 \quad \text{on } Y = 0, 1,$$
$$\text{for } -L_1 < X < L_T - L_1 \tag{5}$$

and the unidirectional, pulsating, flow at the channel inlet is

$$U(-L_1, Y, t) = 1 + A\sin(2\pi St\, t), \quad \text{for } 0 < Y < 1$$
$$V(-L_1, Y, t) = 0. \tag{6}$$

Here, the nondimensional frequency parameter (Strouhal number) St, fH/U_o, is introduced. For the temperature field, the nondimensional fluid inlet temperature is zero:

$$\Theta(-L_1, Y, t) = 0, \quad \text{for } 0 < Y < 1. \tag{7}$$

The upper and lower plates are perfectly insulated:

$$\frac{\partial\Theta}{\partial Y}(X, Y, t) = 0 \quad \text{on } Y = 0, 1,$$
$$\text{for } -L_1 < X < L_T - L_1. \tag{8}$$

Additional downstream boundary conditions are needed owing to the elliptic nature of the governing equations (2)–(4). Neumann conditions for velocity and temperature far downstream can be applied here, assuming fully developed flow and temperature fields. Therefore, the downstream length, L_2, is varied to ensure that the fully developed conditions are not subject to further change.

$$\frac{\partial\Phi}{\partial X}(L_T - L_1, Y, t) = 0, \quad (\Phi = U, V, \Theta),$$
$$\text{for } 0 < Y < 1. \tag{9}$$

In order to solve the above system of equations, the well-established numerical algorithm, SIMPLER of Patankar [12], was employed. As a time integration method, the first-order fully implicit scheme was adopted. For the treatment of the convection terms in equations (2)–(4), a third-order upwind scheme (QUICK) [13] for non-uniform grids was applied. This QUICK scheme avoids substantial numerical diffusions encountered with the usual first-order techniques. Central differencing was used to represent the diffusion transport terms in the governing equations (2)–(4). Finally, the discretized algebraic equations are solved by the tridiagonal matrix algorithm (TDMA).

In the present computations, typically 10–50 iterations were required for the local variables to achieve convergence. For convergence criteria, the relative variations of velocity and temperature between two successive iterations were required to be smaller than the preassigned accuracy levels of 10^{-4}. The residuals of local mass continuity were less than 10^{-8} when a time step was converged. Overall mass continuity through the whole computational domain was satisfied within 10^{-14}. The steady non-pulsating flow results were used as the initial-state conditions to reduce the computational time. In most cases, temporally periodic solutions were obtained after 15–45 cycles of pulsation. The time resolution was such that one pulsating period was divided by 60 time steps during early 5–10 cycles, and then by 120 time steps. The relaxation factors for the variables were set at 1.0 to exclude temporal error during the calculations with 120 time steps a cycle. The relaxation factors used in

the present computations were defined in detail by Patankar [12].

Before proceeding further, it is necessary to ascertain the reliability and accuracy of the present numerical simulations. To this end, quantitative comparisons were made of the reattachment length x_R for steady non-pulsating flow with a parabolic profile, for which experimental data have been documented [14]. Figure 2 demonstrates that the present numerical results are in accordance with available experimental data in the range of $Re < 1000$. It was also found that the discrepancy in the results obtained by using the grids (100×35), (140×50) and (200×70) is smaller than 1%. In addition, the local Nusselt numbers for the case of two-block configuration with (140×50) grids were quantitatively compared to those with (280×100) grids to show the accuracy of the results. Both the results with (140×50) grids and with (280×100) grids displayed a close agreement each other. Based on these test calculations, a grid network of (140×50) was used in all the computations for the two-block configuration. The validation of numerical results for unsteady cases was skipped for conciseness because it can be found in the earlier paper by authors [15].

Also, special concern was given to the grid density in the boundary layer along the solid walls. The boundary layer thickness δ/H from the classical Womersley flow [16] can be assumed as follows:

$$\delta \sim (2\nu/\omega)^{1/2}; \quad \delta/H \sim 1/(St\,Re)^{1/2}. \tag{10}$$

It is noted that the boundary layer thickness becomes much thinner as the Strouhal number is increased. Consequently, spatial grids were clustered to resolve the region of thin boundary layer for high frequency pulsation. Numerical parameters such as time step, grid size, and computational domain, were varied to ensure that the numerical results were essentially independent of the values chosen.

3. RESULTS AND DISCUSSION

In the present calculations, $L_1 = 5.0$ and $L_2 = 29.0$ were used to simulate a long channel. Several sample runs confirmed that these values produced fully-developed flows and satisfied the imposed exit boundary conditions [15, 17]. The blockage ratio h/H, and the length of each block, l/H, were set 0.25 and 1.0, respectively. The Reynolds number Re was varied from 500 to 700. The Prandtl number Pr was set at 0.7 to model air as the working fluid. Emphasis here is placed on the effects of pulsation frequency, i.e. Strouhal number $(0 < St < 2.0)$, the pulsation amplitude $(0.2 < A < 0.7)$, and inter-block spacing w/H $(0.1 < w/H < 5.0)$ on the global flow and heat transfer characteristics.

For comparison purposes, representative velocity and temperature fields around the blocks in the case of a standard non-pulsating flow ($A = 0$) are displayed in Fig. 3. As well understood in Fig. 3(a), the overall flow field may be divided into a mainstream through-flow and recirculating zones. Consequently, heat transfer from the backward-facing surface of the second block as well as the region between the blocks in tandem is least intense since mixing is suppressed in these regions [see Fig. 3(b)]. At subcritical Reynolds number $Re < Re_{crit.}$ (~ 1200), this flow pattern is kept stable. However, by inducing pulsation, this stable and steady flow field can be destabilized, which results in better flow mixing and enhanced thermal transport [6, 7]. Therefore, our interest is in how to determine the better enhancement condition for thermal transport by pulsation.

The influence of pulsation is now manifested. Figure 4 illustrates flow patterns over a cycle at a periodic steady state for $St = 0.4$, $Re = 500$, $A = 0.2$, and $w/H = 1.0$. We can see that recirculating cells are present on the channel walls downstream of the second block. These regularly-spaced vortices are generated from the front corners of the blocks, carried

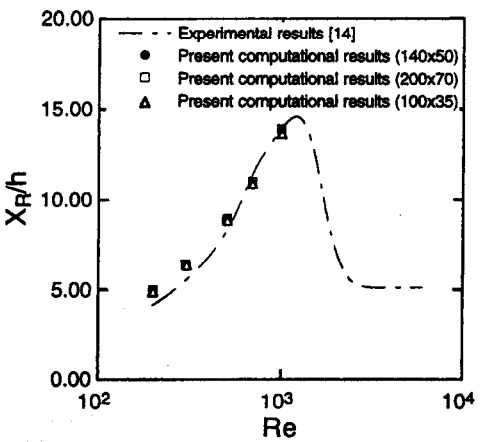

Fig. 2. Comparison of reattachment length as a function of Reynolds number in steady non-pulsating flow for a single block configuration ($w/H = 0.0$). $h/H = 0.25$ and $l/H = 2.0$.

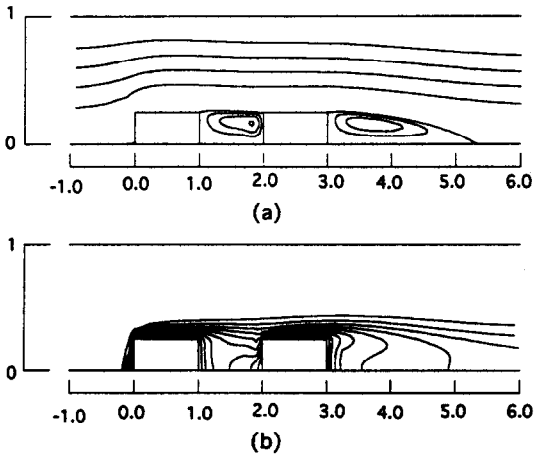

Fig. 3. (a) Streamlines; (b) isotherm contours, for steady non-pulsating flow at $Re = 500$ and $Pr = 0.7$. $\Delta(\Psi/U_iH) = 0.2$ for $0 < (\Psi/U_iH) < 1$ and $\Delta\Theta = 0.1$.

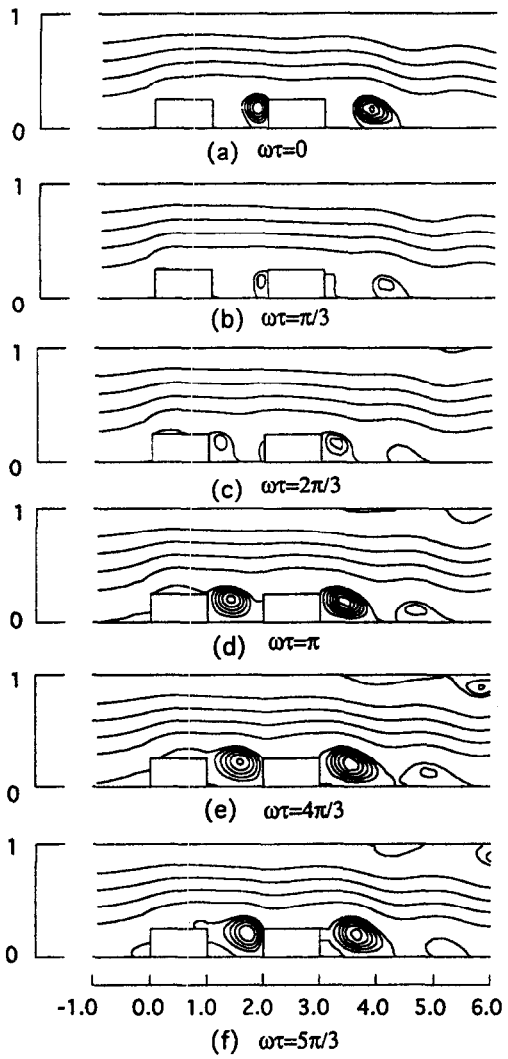

Fig. 4. The variations of streamlines during a cycle at $Re = 500$, $A = 0.2$, $St = 0.4$, and $w/H = 1.0$. $\Delta(\Psi/U_iH) = 0.2$ for $0 < (\Psi/U_iH) < 1$.

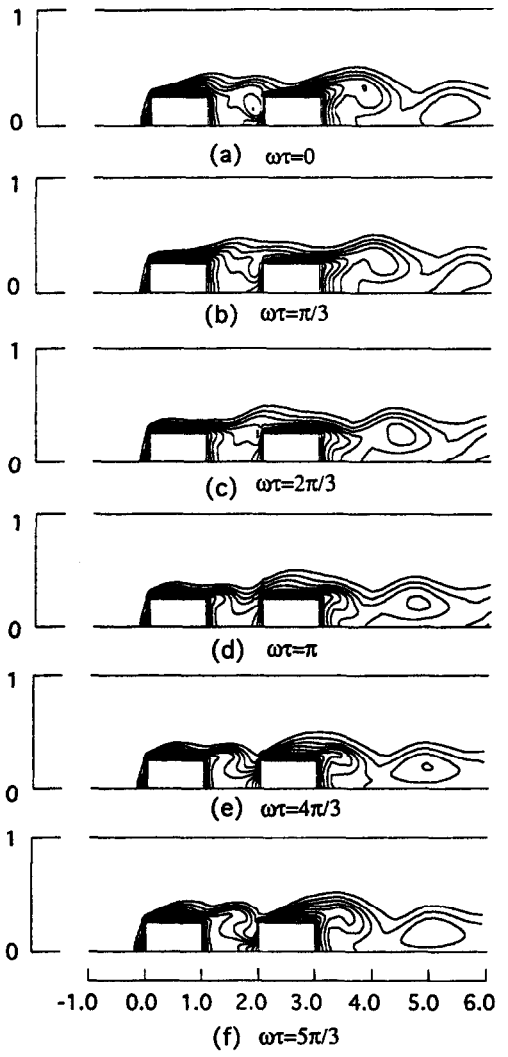

Fig. 5. The variations of isothermal lines during a cycle at $Re = 500$, $Pr = 0.7$, $A = 0.2$, $St = 0.4$, and $w/H = 1.0$, $\Delta\Theta = 0.1$.

downstream of the second block, broken, and finally damped out further downstream. Also, the periodic burst of recirculating cell in the inter-block region during a cycle is noted. This periodic shedding of vortices contributes to the bulk mixing of fluids, particularly in the inter-block region and in the downstream region of the second block.

The impact of pulsation on the thermal field is exhibited in Fig. 5. A spatially wavy pattern, that originates from the front-facing tip of the first block, can also be seen in the downstream region of the second block. Comparison of Fig. 5 with Fig. 3(b) also indicates that the thermal field under a pulsating flow is strongly distorted owing to the presence of periodic shedding of vortices. Note that, as shown in Fig. 5(a)–(c), cold fluids from the mainstream throughflow flow into the enclosed region between the blocks near the front-facing tip of the second block. Note also that a glob of hot fluid, produced from the tip of the hot block, is surrounded by cold fluid in the immediate downstream region of the second block, as shown in Fig. 5(e) and (f). These interactions give rise to the increased heat transport from the block surface to the fluid in the channel.

The influence of wider inter-block spacing w/H on the flow and thermal fields is exhibited in Fig. 6 and 7. In Fig. 6(a)–(c), the vortices generated from the tip of the respective blocks shed downstream in a similar fashion. However, when the vortex initiated from the tip of the first block reaches the front face of the second block, the dominant two recirculating cells of same clock-wise direction are observed inside the inter-block region as seen in Fig. 6(d). The isotherms at the inter-block region show similar patterns compared to those behind the second block as depicted in Fig. 7. This indicates that the thermal interaction between the blocks is weak owing to wider inter-block spacing $w/H = 2.0$, i.e. $w/h = 8.0$.

To obtain an overall measure of transport charac-

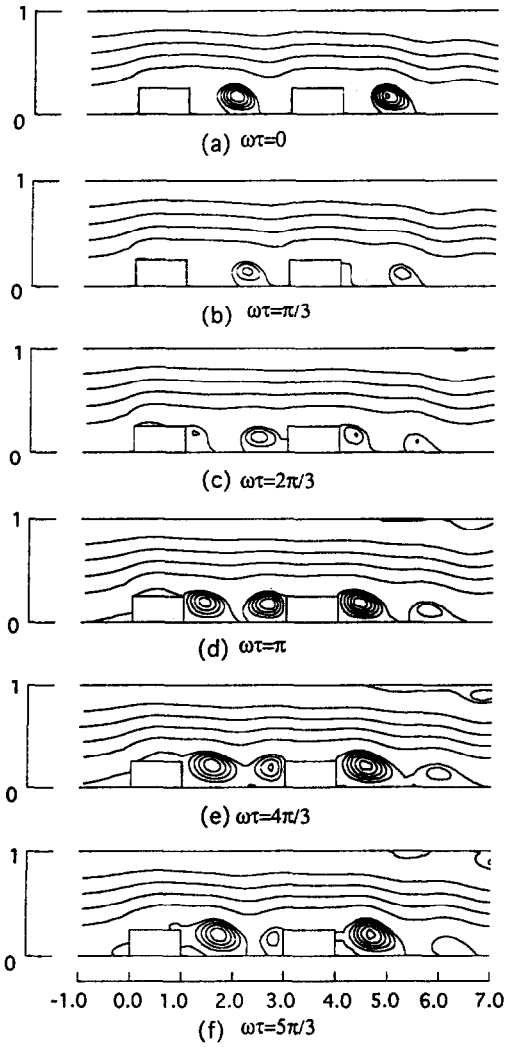

Fig. 6. The variations of streamlines during a cycle at $Re = 500$, $A = 0.2$, $St = 0.4$, and $w/H = 2.0$. $\Delta(\Psi/U_iH) = 0.2$ for $0 < (\Psi/U_iH) < 1$.

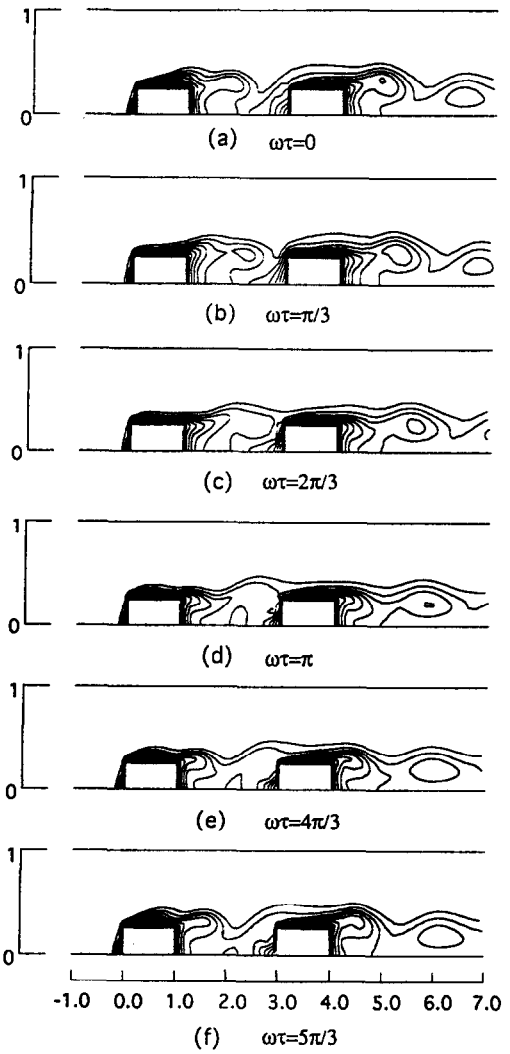

Fig. 7. The variations of isothermal lines during a cycle at $Re = 500$, $Pr = 0.7$, $A = 0.2$, $St = 0.4$, and $w/H = 2.0$. $\Delta\Theta = 0.1$.

teristics of the pulsating flows, the influences of flow pulsation on the heat transfer enhancement factor $\overline{Nu_m}/(Nu_m)_s$, which is normalized by the respective steady non-pulsating value $(Nu_m)_s$, are dealt with in Figs. 9 and 10. First, the Nusselt number $(Nu_m)_s$ for the steady non-pulsating flow is exhibited in Fig. 8. When a steady non-pulsating flow is induced, the $(Nu_m)_s$ of the blocks increases gradually and approaches an asymptotic value, as w/H increases [i.e. $(Nu_m)_s \propto (w/H)^{1/2}$]. This is caused by the increased entrainment of cold fluid into the inter-block region at the wider value of w/H.

Figure 9 demonstrates the effect of the Strouhal number St on the $\overline{Nu_m}/(Nu_m)_s$ for fixed values of $A = 0.2$ and $w/H = 1.0$. Here, abscissa is expressed in log scale to show clearly the effect of St in the range of 0.1–1.0. As St increases, the gain in $\overline{Nu_m}/(Nu_m)_s$ of the first block gradually increases to a maximum around $St \sim 0.8$ as shown in Fig. 9(a), and decreases afterward. For the second block, the appreciable gain

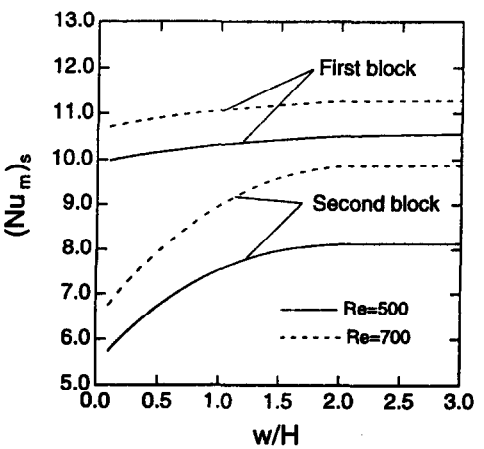

Fig. 8. Plots of space-averaged Nusselt number $(Nu_m)_s$ for the steady non-pulsating flow.

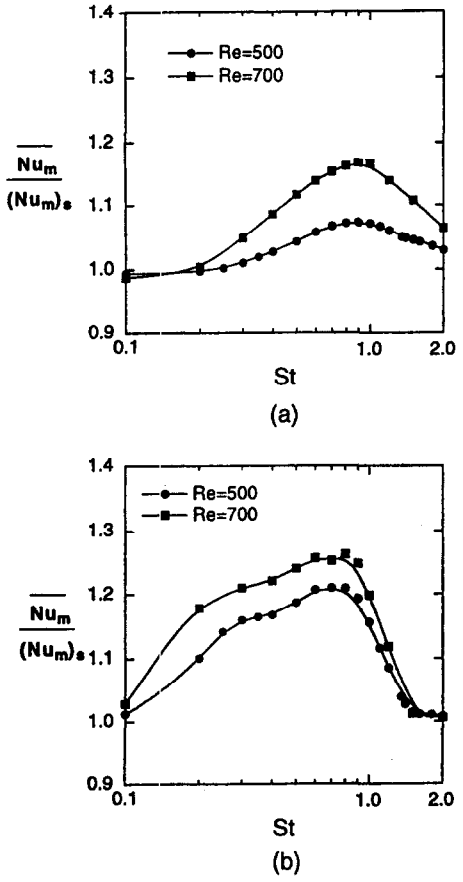

Fig. 9. The effect of Strouhal number St on heat transfer enhancement factor $\overline{Nu_m}/(Nu_m)_s$ at $A = 0.2$ and $w/H = 1.0$. (a) First block; (b) second block.

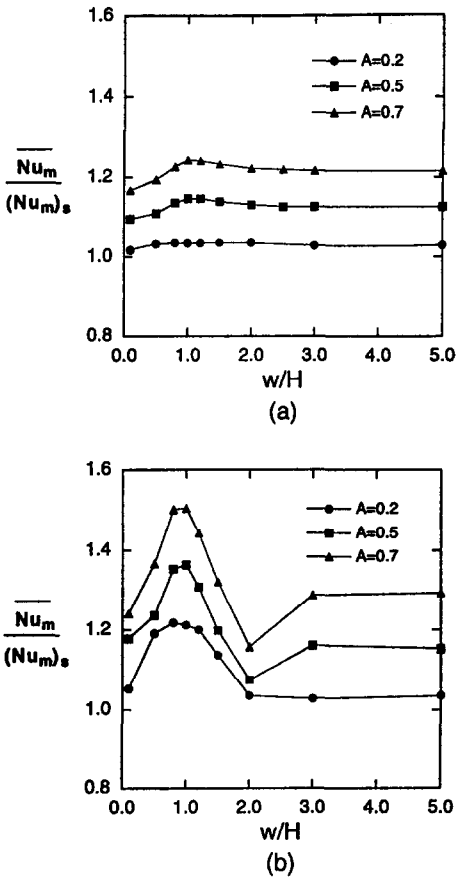

Fig. 10. The effect of spacing w/H on heat transfer enhancement factor $\overline{Nu_m}/(Nu_m)_s$ for various amplitudes A at $St = 0.4$ and $Re = 500$. (a) First block; (b) second block.

in $\overline{Nu_m}/(Nu_m)_s$ is seen at approximately $St \sim 0.8$ in the limited range of St in this study. When the Reynolds number is 500, an increase of about 21% in $\overline{Nu_m}/(Nu_m)_s$ occurs at the frequency of $St \sim 0.8$, and an increase of about 16% at its subharmonic frequency of $St \sim 0.4$. This phenomenon is relevant to the subcritical resonant heat transfer characteristics at a natural shedding frequency of the system. This, in turn, is caused by the active thermal communication between the hot fluid in the inter-block region and the cold fluid in the channel [6]. When the Reynolds number is high ($Re = 700$), the gain in $\overline{Nu_m}/(Nu_m)_s$ is more substantial. This means that the flow is subject to greater destabilization even under identical external pulsation, when the Reynolds number approaches the critical Reynolds number ($Re \rightarrow Re_{crit.}$).

Figure 10 displays the variations of the $\overline{Nu_m}/(Nu_m)_s$ with the inter-block spacing w/H. The Reynolds number Re and the Strouhal number St were fixed at 500 and 0.4, respectively. As w/H increases, the $\overline{Nu_m}/(Nu_m)_s$ has a maximum value of approximately $w/H \sim 1.0$–1.2. The increase in $\overline{Nu_m}/(Nu_m)_s$ is more pronounced at the second block as shown in Fig. 10(b). Therefore, we can say that natural shedding frequency and attendant resonant heat transfer depends closely on the geometric parameter w/H. In addition, the increase of pulsation amplitude A amplifies the resonant heat transfer rate without significantly changing the overall trend in $\overline{Nu_m}/(Nu_m)_s$.

The overall pressure drop Δp throughout the entire channel length is another important quantity. In practical engineering applications, this added pressure drop is the price one pays in return for the gain in heat transfer augmentation by inducing pulsation. The dimensionless pressure drop can be expressed in the friction factor f_p:

$$f_p \equiv \frac{(-\Delta p/l_T) \cdot D_h}{\rho U_o^2/2} \tag{11}$$

where, D_h $(=2H)$ is the hydraulic diameter of the channel. Figures 11 and 12 show the effects of St and w/H on the instantaneous friction factor $f_p/(f_p)_s$, respectively. In Fig. 11, the amplitude of the fluctuating friction factor substantially increases, as St increases. However, the magnitude of the instantaneous friction factor is less affected by the change of w/H, as seen in Fig. 12. The effect of pulsating amplitude A on the friction factor $f_p/(f_p)_s$ is also displayed in Fig. 13. When A is large, as expected, the $f_p/(f_p)_s$ increases dramatically. The cycle-averaged

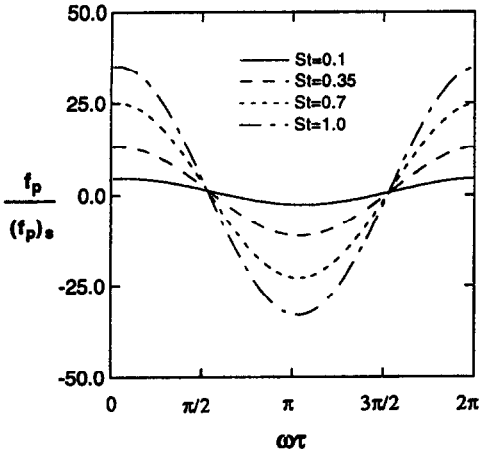

Fig. 11. The temporal variations of friction factor f_p for various St at $Re = 500$, $w/H = 1.0$ and $A = 0.2$.

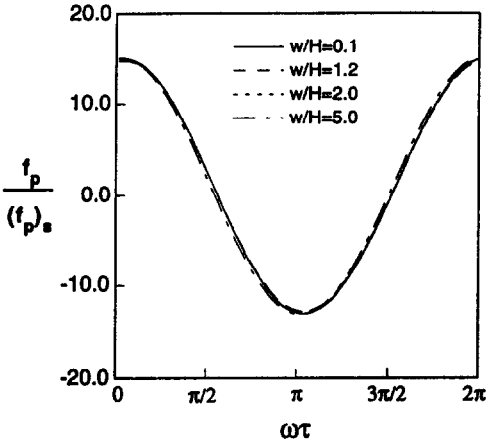

Fig. 12. The temporal variations of friction factor f_p for various w/H at $Re = 500$, $A = 0.2$ and $St = 0.4$.

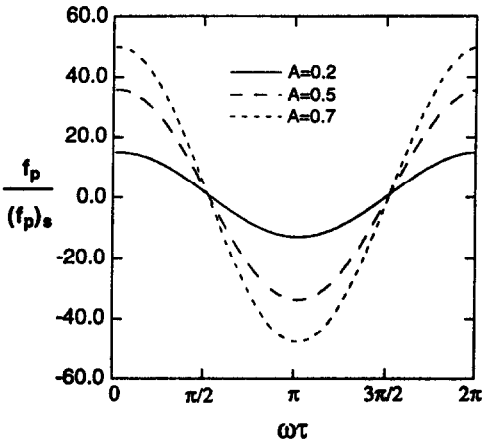

Fig. 13. The temporal variations of friction factor f_p for various A at $Re = 500$, $w/H = 2.0$ and $St = 0.4$.

friction factors $\overline{f_p}$ are slightly larger than the steady non-pulsating friction factor $(f_p)_s$. The phase leads of $f_p/(f_p)_s$ over the inlet pulsating velocity are nearly $\pi/2$. This indicates that the flow pulsation considered in this study occupies a high frequency regime, when compared to the Womersley flow inside a smooth duct (i.e. $St = 2\pi\beta^2/Re$, where $\beta \equiv H(\omega/\nu)^{1/2}$ the Womersley number) [16].

In order to investigate the contribution of fluctuating components in velocity and temperature on heat transfer, the correlations between velocity and temperature will be dealt with. Figure 14 exemplifies the contour plots of Reynolds stress (additional momentum diffusion) $-\rho\overline{u'v'}$ and Reynolds heat flux (additional convection) $\rho C_p\overline{v'T'}$. Reynolds stress plays a dominant role in mean momentum transfer by flow fluctuation such as turbulent flow [18]. As clearly depicted in Fig. 14(a), most of the portions near the upper and the backward faces of the blocks are occupied by the positive values of $-\overline{U'V'}$. This means that the flow mixing is substantially increased in the mixing-suppressed regions for the steady non-pulsating flow. Also, the substantial increase of $\overline{V'\Theta'}$ in these regions is germane to the enhanced thermal transport by flow pulsation, as seen in Fig. 14(b).

Figures 15(a) and (b) show phase diagrams of U vs V and V vs Θ at a monitoring point $(x, y) = (l_1 + w/2, h/2)$, respectively. The phase diagrams of U vs V and V vs Θ display a simple closed loop with higher harmonics. It should be noted that the well-closed loops for all cases of Strouhal numbers clearly indicate that the flow and thermal field is in a highly time-periodic regime. Therefore, it can be distinguished from turbulent flow, which shows a random chaotic motion. Thus, we can learn more by decomposing the fluctuating velocities and temperature by Fourier-series representations [15, 17].

$$u_i' = \sum_{n=1}^{\infty} (u_i)_n \cdot \sin\left[n\omega\tau + (\phi_i)_n\right] \tag{12}$$

$$T = \sum_{n=1}^{\infty} (T)_n \cdot \sin\left[n\omega\tau + (\phi_T)_n\right] \tag{13}$$

where ϕ_n reflects the phase advances of the nth component relative to the inlet velocity. The $(u_i)_n$ and

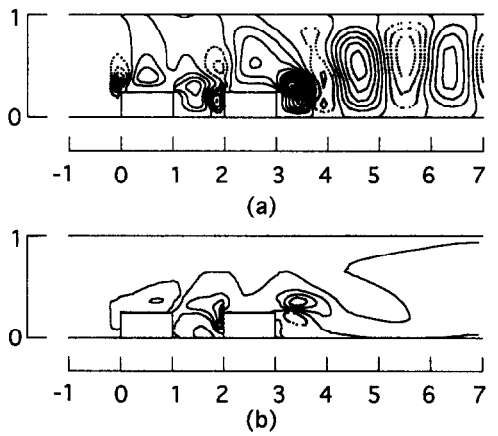

Fig. 14. Contour plots of $-\overline{U'V'}$ (a) and $\overline{V'\Theta'}$ (b). $Re = 500$, $St = 0.4$ and $w/H = 1.0$. (a) $\Delta(-\overline{U'V'}) = 0.005$; (b) $\Delta(\overline{V'\Theta'}) = 0.005$. The dotted lines indicate negative values.

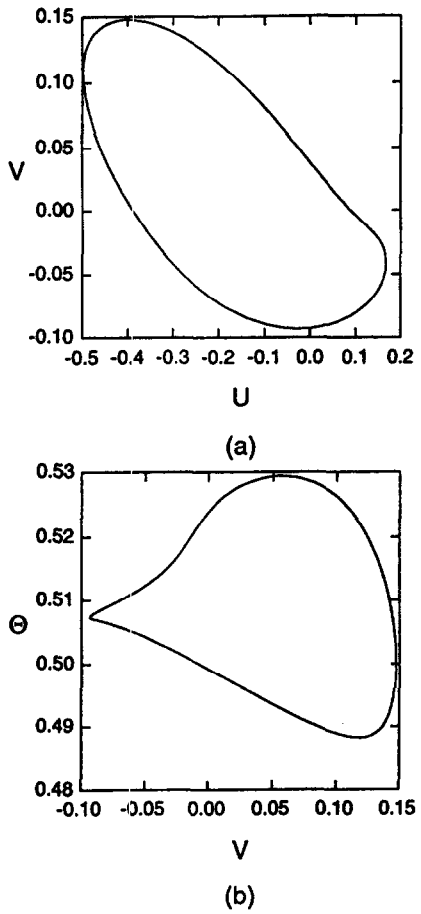

Fig. 15. Phase diagrams of U vs V (a) and V vs Θ (b) at $(x, y) = (l_1 + w/2, h/2)$. $Re = 500$, $w/H = 1.0$, $A = 0.2$ and $St = 0.4$.

$(T)_n$ represent the magnitude of the nth harmonic fluctuations of u, v and T, respectively. When the above relations are substituted in Reynolds stress $-\rho\overline{u_i'v_j'}$ and Reynolds heat flux $\rho C_p\overline{u_i'T'}$, they yield

$$-\rho\overline{u_i'v_j'} = -\rho\sum_{n=1}^{\infty}\frac{(u_i)_n\cdot(u_j)_n}{2}\cos[(\phi_i)_n-(\phi_j)_n] \quad (14)$$

$$\rho C_p\overline{u_i'T'} = \rho C_p\sum_{n=1}^{\infty}\frac{(u_i)_n\cdot(T')_n}{2}\cos[(\phi_i)_n-(\phi_T)_n]. \quad (15)$$

It is interesting to note that $-\rho\overline{u_i'v_j'}$ and $\rho C_p\overline{u_i'T'}$ mainly depend on the magnitude of the nth fluctuating components and the phase differences between the nth 'tuned' fluctuating components of the variables. Basically, the nonlinear interactions due to the fluctuating components give rise to a substantial increase of $-\rho\overline{u_i'v_j'}$ and $\rho C_p\overline{u_i'T'}$ in the vicinity of heated blocks. These increases, by flow pulsation, contribute significantly to momentum diffusion, i.e. better flow mixing, and, eventually, to enhanced convective heat transfer.

4. CONCLUSION

A numerical study was carried out for pulsating flow and the associated heat transfer from two successive, heated, blocks inside a channel. Findings indicate that, by pulsation, a steady and stable flow field is substantially destabilized and exhibits a regularly-spaced vortex shedding behind the last block. Phase-diagrams also indicate that this unsteady pulsating flow is highly periodic and well-organized. The temperature field is substantially affected by such increased large-scale flow mixing. The heat transfer enhancement factor $\overline{Nu_m}/(Nu_m)_s$ of the blocks shows a dominant peak as St varies. When the Reynolds number is high, the gain in $\overline{Nu_m}/(Nu_m)_s$ is more pronounced at the second block. This trend shows a relevance to the natural shedding frequency of the system. It is also evident that a favorable condition for heat dissipation exists in the thermal system due to changes in spacing w/H, since the natural shedding frequency strongly depends upon w/H. The increase of pulsation amplitude A significantly augments the overall heat transfer rate.

The results of this investigation clearly indicate that the flow pulsation induced at the channel inlet can be utilized to enhance heat transport in thermal systems. However, one must consider a tolerance limit in view of increased pressure drop and to determine the optimal frequency of external pulsation according to the geometrical parameter w/H.

Acknowledgements—The authors acknowledge the support of Korea Institute of Science and Technology through Grant no. 2N13603 for this work.

REFERENCES

1. Kraus, A. D. and Bar-Cohen, A., *Thermal Analysis and Control of Electronic Equipment*. Hemisphere, New York, 1983.
2. Davalath, J. and Bayazitoglu, Y., Forced convection cooling across rectangular blocks. *Transactions of ASME Journal of Heat Transfer*, 1987, **109**, 321–327.
3. Kang, B. H., Jaluria, Y. and Tewari, S. S., Mixed convection transport from an isolated heat source module on a horizontal plate. *Transactions of the ASME Journal of Heat Transfer*, 1990, **112**, 653–661.
4. Kim, S. Y., Sung, H. J. and Hyun, J. M., Mixed convection from multiple-layered boards with cross-streamwise periodic boundary conditions. *International Journal of Heat Mass Transfer*, 1992, **35**, 2941–2952.
5. Ghaddar, N. K., Korczak, K. Z., Mikic, B. B. and Patera, A. T., Numerical investigation of incompressible flow in grooved channels. Part 1. Stability and self-sustained oscillations. *Journal of Fluid Mechanics*, 1986, **163**, 99–127.
6. Ghaddar, N. K., Magen, M., Mikic, B. B. and Patera, A. T., Numerical investigation of incompressible flow in grooved channels. Part 2. Oscillatory heat transfer enhancement. *Journal of Fluid Mechanics*, 1986, **168**, 541–567.
7. Greiner, M., An experimental investigation of resonant heat transfer enhancement in grooved channel. *International Journal of Heat and Mass Transfer*, 1991, **34**, 1383–1391.
8. Amon, C. H. and Mikic, B. B., Spectral element simulations of unsteady forced convective heat transfer:

Application to heat exchanger geometries. *Numerical Heat Transfer*, 1991, **19,** 1–19.
9. Azar, K., Enhanced cooling of electric components by flow oscillation. *Journal of Thermophysics Heat Transfer*, 1992, **6,** 700–706.
10. Suzuki, K., Xi, G. N., Inaoka, K. and Hagiwara, Y., Mechanism of heat transfer enhancement due to self-sustained oscillation for in-line fin array. *International Journal of Heat and Mass Transfer*, 1994, **37,** 83–96.
11. Drazin, P. G. and Reid, W. H., *Hydrodynamic Stability*. Cambridge University Press, Cambridge, 1981.
12. Patankar, S. V., *Numerical Heat Transfer and Fluid Flow*. Hemisphere, New York, 1980.
13. Hayase, T., Humphrey, J. A. C. and Grief, R., A consistently formulated QUICK scheme for fast and stable convergence using finite-volume iterative calculation procedures. *Journal of Computational Physics*, 1992, **98,** 108–118.
14. Tropea, C. D. and Gackstatter, R., The flow over two-dimensional surface-mounted obstacles at low Reynolds numbers. *Transactions of the ASME Journal of Fluids Engineering*, 1985, **107,** 489–494.
15. Kim, S. Y., Kang, B. H. and Hyun, J. M., Heat transfer in the thermally developing region of a pulsating channel flow. *International Journal of Heat and Mass Transfer*, 1993, **36,** 4257–4266.
16. Schlichting, H., *Boundary-layer Theory*. McGraw-Hill, New York, 1979.
17. Kim, S. Y., Kang, B. H. and Hyun, J. M., Convection from a rectangular heated block in pulsating channel flow. *Proceedings of the 10th International Heat Transfer Conference*, Brighton, U.K., Vol. 4, 1994, 267–272.
18. Tennekes, H. and Lumley, J. L., *A First Course in Turbulence*. MIT Press, Michigan, 1992.